Hindawi
Journal of Electrical and Computer Engineering
Volume 2024, Article ID 9760875, 1 page
https://doi.org/10.1155/2024/9760875

Retraction

Retracted: Research on Optimal Control Method of Tennis Racket String Diameter Based on Kalman Filter Algorithm

Journal of Electrical and Computer Engineering

Received 23 January 2024; Accepted 23 January 2024; Published 24 January 2024

This article has been retracted by Hindawi following an investigation undertaken by the publisher [1]. This investigation has uncovered evidence of one or more of the following indicators of systematic manipulation of the publication process:

(1) Discrepancies in scope

(2) Discrepancies in the description of the research reported

(3) Discrepancies between the availability of data and the research described

(4) Inappropriate citations

(5) Incoherent, meaningless and/or irrelevant content included in the article

(6) Manipulated or compromised peer review

The presence of these indicators undermines our confidence in the integrity of the article's content and we cannot, therefore, vouch for its reliability. Please note that this notice is intended solely to alert readers that the content of this article is unreliable. We have not investigated whether authors were aware of or involved in the systematic manipulation of the publication process.

Wiley and Hindawi regrets that the usual quality checks did not identify these issues before publication and have since put additional measures in place to safeguard research integrity.

We wish to credit our own Research Integrity and Research Publishing teams and anonymous and named external researchers and research integrity experts for contributing to this investigation.

The corresponding author, as the representative of all authors, has been given the opportunity to register their agreement or disagreement to this retraction. We have kept a record of any response received.

References

[1] X. Chen, "Research on Optimal Control Method of Tennis Racket String Diameter Based on Kalman Filter Algorithm," *Journal of Electrical and Computer Engineering*, vol. 2022, Article ID 9356608, 14 pages, 2022.

Hindawi
Journal of Electrical and Computer Engineering
Volume 2022, Article ID 9356608, 14 pages
https://doi.org/10.1155/2022/9356608

Research Article

Research on Optimal Control Method of Tennis Racket String Diameter Based on Kalman Filter Algorithm

Xin Chen

Shenyang Jianzhu University, Shenyang 110168, China

Correspondence should be addressed to Xin Chen; 1073907651@sjzu.edu.cn

Received 12 February 2022; Revised 2 March 2022; Accepted 11 March 2022; Published 2 May 2022

Academic Editor: Wei Liu

In order to explore the optimal control method of tennis racket string diameter, this paper applies the Kalman filter algorithm to the collection and processing of tennis sports parameters. When the Kalman filter uses the optimal gain (the Kalman filter enters the steady state), the corresponding cost function is established based on the noncorrelated nature of its residual sequence, which is used as the judgment condition for the sampling strategy switch to improve the stability of the system. In addition, this paper improves the real-time performance and calculation accuracy of data transformation through adaptive sampling strategy and adaptive scale factor, improves the stability and estimation accuracy of the system as a whole, and builds an intelligent monitoring system. Finally, this paper systematically studied the optimization control method of tennis racket string diameter and verified that the Kalman filter algorithm can play a certain role in the optimization control of tennis racket string diameter.

1. Introduction

In recent years, with the popularity of tennis in our country, more and more people have participated in this sport, which has enabled tennis to develop rapidly in our country. However, the sport of tennis in my country is relatively young, started relatively late, has a poor mass base, and has low social popularity. Therefore, a large amount of tennis expertise and professionals are urgently needed to promote its development. At present, the research on tennis mainly focuses on the technical movements of tennis and the physical fitness of players, and there is little research on tennis rackets. However, in tennis, the impact of the racket on the participants is very obvious. How to choose a suitable racket plays a very important role in improving the level of sports and reducing sports injuries.

After more than one hundred years of development, tennis has become a popular sport all over the world. Like other sports, the development of new materials has a profound impact on tennis, especially the design of tennis rackets. The tennis racket has changed from the original wooden racket frame to the current various alloys and graphite carbon fiber materials, which greatly reduces the weight of the tennis racket, changes the position of the center of mass and the moment of inertia of the tennis racket, and increases the stiffness characteristics of the racket [1]. Moreover, the material of tennis racket strings has also developed from the original natural animal gut to the current chemical polymers such as polyester fiber and Kevlar fiber. The change of string material affects the tension of the racket surface, the coefficient of friction, the modulus of elasticity, etc. [2]. The development of technology has made the tennis racket lighter and stronger, and the racket surface more flexible. These will affect the speed and angle of the serve, the impact force of the racket, the deformation of the racket surface, the energy storage, etc. and then affect the tennis player's use of skills in the course of tennis. At the same time, changes in tennis rackets have also brought new sports injuries to athletes. In tennis, common injuries are caused by the collision force and vibration generated by the collision of the tennis ball and the racket to the upper limbs. Typical tennis sports injuries include sprains of the wrist, elbow, shoulder, waist, knee and ankle joints, and muscle and ligament strains. In particular, it is more likely to cause injury when the technical actions are not standardized or excessively distributed.

Based on the above analysis, this paper combines the Kalman filter algorithm to study the optimization control method of tennis racket string diameter and improves the research effect through the intelligent simulation system.

2. Related Work

Literature [3] uses three-dimensional high-speed video and video analysis methods, using the principles and methods of sports biomechanics, to test and analyze the vigorous serve technique of outstanding female tennis players and make a diagnosis and evaluation of the rationality of the subjects' movement techniques. Literature [4] used a capacitive grip sensor to test the grip strength of 15 subjects during a shot and found that the change in grip strength had no effect on the speed of the ball in all the impact areas of the racket surface. Literature [5] used the same method to test 19 professional athletes and 13 amateur high-level athletes and found that although professional athletes have faster ball speeds, there is no difference in grip strength between professional athletes and amateur high-level athletes. The maximum grip strength of the two groups did not occur when the ball was in contact with the string but about 30 ms before the ball was hit. The change of grip size will also have an impact on the ball speed. Literature [6] tested on subjects of different genders and levels and found that, in soft tennis forehands, gender and level have an effect on the strength of the ball. Influential, professional athletes with greater grip strength and long middle fingers will increase the power and speed of the ball as the grip size increases when hitting the ball. While the force exerted by the human body on the racket and the size of the grip have different effects on the speed of the ball, the contact position of the ball and the racket surface also has an effect on the speed of the ball. Literature [7] believes that the speed of the ball in the dessert area is the fastest when hitting the ball. Literature [8] believed that the swing of the racket increases the speed of the far end hitting point, which in turn increases the speed of the ball.

Literature [9] pasted a capacitive grip sensor on the grip and an acceleration sensor on the wrist to test the impact of grip changes on the vibration of the racket to the body. The speed hits the marked area and the nonmarked area. Analysis of the obtained data found that, in all the impact areas, the greater the grip strength on the grip, the greater the vibration transmitted to the arm, the grip strength is reduced, and the vibration load on the arm is reduced. Literature [10] uses regression analysis to explain the relationship between longitudinal collision position and ball speed, vibration, and arm vibration. The subjects of the experiment were 19 professional athletes. Acceleration sensors were attached to the athletes' elbows, wrists, and racket neck positions, allowing the athletes to make 30 forehand and backhand shots to measure the contact points between the ball and the racket surface. Regression analysis found that the vibration of the arms of all subjects during the hitting process increased significantly as the hitting point moved from the racket head near the grip position to the farthest end of the racket head, and the contact position between the ball and the racket surface. There is an obvious secondary correlation with vibration. In literature [11], through static research (the subject holds the racket to keep the batting posture, and the ball hits the racket surface at a certain speed) and test and analysis of the test data, it is found that the vibration frequency of the clap hand is 0–120 Hz, for the shock absorber. Compared with the impact analysis without shock absorbers, the amplitude of the wrist and elbow is not significantly different. The collision in the nonsweet area produces greater amplitude. The amplitude of the nonsweet area is 5 times the amplitude of the sweet area, but this is not the same as the avoidance. There is no correlation between the shock device and the location of the impact. During the impact, the shock absorber had no effect on grip strength and forearm electromyography. Literature [12] studies the impact of string stiffness on forearm muscle fatigue. Through statistical analysis of the speed of the ball hitting the ball and the acceleration of the frame during collision, it is found that the string with high stiffness produces a peak acceleration of 5060 when hitting the ball ±1892 m/s2, the vibration frequency of the frame is 204 ± 29 Hz, the acceleration peak of the string with low hardness at hitting the ball is 4704 ± 1671 m/s2, the vibration frequency of the frame is 191 ± 16 Hz, and the string with high hardness is used. After the game, the maximum forearm grip strength is reduced by 15%, and the forearm grip strength will not change significantly after the game is finished using a string with a low rigidity. The increase in forearm fatigue may be caused by the increase in grip strength in order to maintain the stability of the racket during the collision of the ball with the racket surface.

In literature [13], in the electromyographic analysis of the forehand stroke, the brachioradialis muscle of the forearm is selected as the target muscle, and the integrated electromyographic analysis on it shows that the brachioradialis muscle plays a role in the forehand stroke. However, the role of brachioradialis in the results of the study is not obvious. According to the function of the brachioradialis muscle in the anatomy and the technical movements of the tennis forehand, it is found that this research conclusion is not scientific. Literature [14] studied the characteristics of the surface EMG when the forehand muscle exerts force. The integrated EMG was used to analyze the brachioradialis muscle of the forearm and believed that the brachioradialis muscle was one of the main muscles in the forehand shot. Literature [15] studied the electromyographic characteristics of forehand shots and found that the flexor carpi ulnaris is one of the key muscles for accelerating straight forehand shots and accelerating slash forehand shots in forehand shots.

Literature [16] made some summary of serve and net tactics. It made some conclusions about when they came to the net, how to receive and receive the serve, how to use combination tactics to create net opportunities, and how to use net tactics when the score is leading or lagging, incisive exposition.

3. Improvement of Kalman Filter Algorithm

The main problems of UT transform sampling strategy are as follows. The distance between the i-th Sigma point χ_i and $\widehat{x}$ is $\widehat{x}$, which is proportional to $\sqrt{(L+\kappa)}$. As the dimensionality

of the state space increases, the radius of the sphere formed by the Sigma point continues to increase, which in turn leads to nonlocal sampling. For some strong nonlinear problems, the filtering accuracy will decrease or even diverge. The scale factor selection $K = 3 - L$ can eliminate the influence of the dimension on the distance to a certain extent. However, when the dimensionality is higher than 3, it will cause the calculated covariance to be nonpositive semidefinite. Based on this, the initial Sigma point set needs to be scaled up. At present, proportional symmetric sampling is commonly used, and the process is as follows:

Considering that the mean and covariance of the state space vector X are $\widehat{x}$ and P_{xx}, respectively, $\widehat{x}$ and P_{xx} are approximated by 2L + Z Sigma points, and the Sigma point set is obtained as follows:

$$\chi_{k-1} = \left[\widehat{X}_{k-1}, \widehat{X}_{k-1} + \left(\sqrt{(L+\lambda)P_{X,k-1}}\right), \widehat{X}_{k-1} - \left(\sqrt{(L+\lambda)P_{X,k-1}}\right)\right]. \tag{1}$$

In the formula, $\lambda = \alpha^2 \cdot (L + \kappa) - L$, $(\sqrt{(L+\lambda)P_{X,k-1}})$ which means the i-th column of the square root of matrix $(L + \lambda)P$, and the corresponding sampling point weight is

$$\begin{cases} w_0^{(m)} = \dfrac{\lambda}{(L+\lambda)}, \\ w_0^{(c)} = \dfrac{\lambda}{(L+\lambda)} + \left(1 - \alpha^2 + \beta\right), \\ w_i^{(m)} = w_i^{(c)} = \dfrac{1}{(2(L+\lambda))}; \quad i = 1 \sim 2L, \\ w_0^{(c)} = \dfrac{\lambda}{(L+\lambda)} + \left(1 - \alpha^2 + \beta\right), \\ w_i^{(m)} = w_i^{(c)} = \dfrac{1}{(2(L+\lambda))}; \quad i = 1 \sim 2L. \end{cases} \tag{2}$$

In the formula, κ is a proportional parameter, which adjusts the distance between the Sigma point and the mean $\widehat{x}$. The parameter mainly affects the error caused by higher-order moments above the second order. For the Gaussian distribution, its value is generally 3-L.

We set χ_i^j to be the i-th sampling point in the Sigma point set in the j-dimensional space, $\widehat{x}$ is the center point, and P_{xx} is the covariance. Then, the n-dimensional minimum skewness sampling is as follows:

(1) The algorithm selects W_0, and the value range is [0, 1].

(2) The algorithm calculates the weight of sigma points, and considering the center point, the number of sigma points is $L + 2$.

$$W_i = \begin{cases} \dfrac{1 - W_0}{2^n}, & i = 1, 2, \\ 2^{i-1} W_1, & i = 3, \ldots, L. \end{cases} \tag{3}$$

(3) The algorithm initializes the iteration vector (when the state is one-dimensional).

$$\begin{aligned} \chi_0^1 &= [0], \\ \chi_1^1 &= \left[-\frac{1}{\sqrt{2W_1}}\right], \\ \chi_2^1 &= \left[\frac{1}{\sqrt{2W_1}}\right]. \end{aligned} \tag{4}$$

(4) When the input dimension is $j = 2, \ldots, n$, the iterative formula is

$$\chi_i^{j+1} = \begin{cases} \begin{bmatrix} \chi_0^j \\ 0 \end{bmatrix}, \\ \qquad\qquad , \quad i = 1, \ldots, j. \\ \begin{bmatrix} \chi_i^j & -\dfrac{\sqrt{2W_{j+1}}}{\sqrt{2W_{J+1}}} \\ 1 & \end{bmatrix} \end{cases} \tag{5}$$

(5) The algorithm adds the mean and covariance information of X to the generated Sigma point set, and we can get

$$\chi_i = \widehat{x} + \alpha \cdot \sqrt{P_{xx}} \chi_i^j. \tag{6}$$

In the formula, $\sqrt{P_{xx}}$ is the square root matrix of P_x, which is calculated by Cholesky decomposition method. If $P_{xx} = SS^T$, then $\sqrt{P_{\mathrm{sx}}} = S$.

In the minimum skewness simplex sampling strategy, as the dimension increases, the influence of higher-order errors also increases. The basis embeds the proportional UT transform into the minimum skewness simplex sampling, and its expression is as follows:

$$W_i^m = \begin{cases} \dfrac{W_0}{\alpha^2} + \left(1 - \dfrac{1}{\alpha^2}\right), & i = 0, \\ \dfrac{1 - W_0}{2^n \cdot \alpha^2}, & i = 1, 2, \\ \dfrac{2^{i-2} \cdot W_1}{\alpha^2}, & i = 3, \ldots, L + 1, \end{cases} \tag{7}$$

$$W_i^c = \begin{cases} W_0^m + \left(1 + \beta - \alpha^2\right), & i = 0, \\ W_i^m, & i \neq 0. \end{cases}$$

In the formula, W_i^n and W_i^c are the weights of the mean and covariance of the system state vector in the unscented transformation, respectively. The scale factor α controls the distance from the Sigma point to the mean value of the center point. By controlling the value of α, "nonlocal effects" can be effectively avoided. If the system obeys the Gaussian distribution, the value of β is the optimal value.

The hypersphere simplex sampling uses $L+2$ sampling points to match the second moment information of the sample variables. The distance from the sigma point to the central mean point is the same, and the corresponding weights are also equal. The Sigma point set presents a hypersphere shape in spatial distribution, which is why this sampling strategy is called hypersphere simplex sampling. The resulting Sigma points are as follows:

(1) The algorithm selects W_0, and the value range is [0, 1].

(2) The algorithm calculates the weights of Sigma points.

$$W_i = (1 - W_0)(L + 1). \tag{8}$$

(3) The algorithm initializes the iteration vector (when the state is one-dimensional).

$$\begin{aligned} \chi_0^1 &= [0], \\ \chi_1^1 &= \left[-\frac{1}{\sqrt{2W_1}} \right], \\ \chi_2^1 &= \left[\frac{1}{\sqrt{2W_1}} \right]. \end{aligned} \tag{9}$$

(4) When the input dimension is $j = 2, \ldots, L$, the iterative formula is

$$\chi_i^{j+1} = \begin{cases} \begin{bmatrix} \chi_0^j \\ 0 \end{bmatrix}, & i = 0, \\ \begin{bmatrix} \chi_i^{j-1} \\ 1 \\ \dfrac{\sqrt{j(j+1)W_1}}{\sqrt{2}} \end{bmatrix}, & i = 1, \ldots, j, \\ \begin{bmatrix} 1 \\ 0 \\ \sqrt{j(j+1)W_1} \end{bmatrix}, & i = j + 1. \end{cases} \tag{10}$$

(5) The algorithm adds the mean and covariance information of X to the generated Sigma point set, and we can get

$$\chi_1 = \widehat{x} + \sqrt{P_x}\chi_i^j. \tag{11}$$

The scale factor α mainly affects the distance from the Sigma point to the center point $\widehat{x}$, and the effect of controlling the distance from the Sigma point to the center point can be achieved by adjusting the value of α. In order to avoid "nonlocal effects," we usually need to control the value of α within a certain range. In addition, the scale factor α can also affect the error of higher-order terms. Substituting the Sigma point obtained after UT transformation into the state function, we can get

$$y = f(\widehat{x} + \alpha(x - \widehat{x})). \tag{12}$$

Carrying out Taylor expansion of the functional formula at $\widehat{x}$, we can get

$$\begin{aligned} y = f(\widehat{x}) + \frac{f(\widehat{x})}{1!}\alpha(x - \widehat{x}) + \frac{f'(\widehat{x})}{2!}\alpha^2(x - \widehat{x})^2 \\ + \cdots\cdots + \frac{f^{(n)}(\widehat{x})}{n!}\alpha^n(x - \widehat{x})^n + R_n(x), \end{aligned} \tag{13}$$

$$\begin{aligned} \widehat{y} = E[y] = f(\widehat{x}) + \frac{1}{2}(x - \widehat{x})^2 P_{xx} \\ + \frac{1}{6}(x - \widehat{x})^3 E\left[\alpha x^3\right] + \cdots\cdots, \end{aligned} \tag{14}$$

$$\begin{aligned} P_{yy} &= E\left[(y - \widehat{y})(y - \widehat{y})^T\right] \\ &= (x - \widehat{x})P_{yx}(x - \widehat{x})^T + \frac{1}{2}(x - \widehat{x})^2 E\left[\alpha x^3\right](x - \widehat{x})^T \\ &\quad + \frac{1}{2}(x - \widehat{x})E\left[\alpha x^3\right]\left((x - \widehat{x})^2\right)^T \\ &\quad + \frac{1}{2}(x - \widehat{x})^2\left(E\left[\alpha x^4\right] - E\left[\alpha x^2 P_y\right] - E\left[P_{yy}\alpha x^2\right]\right. \\ &\quad \left. + P_{yy}^2\right)\left((x - \widehat{x})^2\right)^T \\ &\quad + \frac{1}{6}(x - \widehat{x})^3 E\left[\alpha x^4\right](x - \widehat{x})^T + \cdots. \end{aligned} \tag{15}$$

It can be seen from (14) and (15) that the scale-corrected UT transformation has reached the second-order truncation accuracy for the transmission of the system measurement mean and the covariance matrix $\widehat{y}$ and P_{yy}. By controlling the value of α to control the error of higher-order terms, to meet the accuracy requirements of the actual system state estimation, the scale factor β is used to introduce the prior information of the distribution of random variables x. If the random variable x obeys the normal distribution, the value of β is 2, which is the best, and the combination factor of $(1 - \alpha^2 + \beta)$ ensures the semipositive definiteness of the predictive covariance matrix.

In an actual system, random state jumps and parameter drift will adversely affect the performance and stability of the filtering algorithm. In this case, the algorithm needs to have good real-time performance and timely feedback processing. When the system reaches a steady state, the Kalman filter is already in a corresponding steady state. At this time, the algorithm's requirements for accuracy are increased, so the corresponding sampling accuracy requirements are increased. Based on this, adjusting the sampling strategy according to system state changes is a way to improve the stability of the Kalman filter.

The corresponding cost function can be established according to the noncorrelated nature of the residual sequence of the Kalman filter when the optimal gain is used (the Kalman filter enters the steady state), which can be used as the judgment condition for the switching of the sampling strategy. The specific formula is as follows:

$$\varepsilon_k \cdot \varepsilon_k^T \le tr\left[E\left(\varepsilon_k \cdot \varepsilon_k^T\right)\right]. \tag{16}$$

In the formula, the residual sequence $\varepsilon_k = z_k - h(\hat{x}_k, v_k)$, z_k is the measured value at time k, $h(\bullet)$ is the transfer function of the system measurement equation, and v_k is the measured noise at time k. The left side of the inequality is the sum of squares of the residuals, which includes the factors of the actual estimation error. We apply the judgment condition to the unscented Kalman filter algorithm, and the process is as follows:

(1) The algorithm initializes it as follows:

$$\begin{aligned} \hat{x}_0 &= E[x_0], \\ P_0 &= E\left[(x_0 - \hat{x}_0) \cdot (x_0 - \hat{x}_0)^T\right]. \end{aligned} \tag{17}$$

The algorithm selects the minimum skewness monomorphic sampling as the initial sampling policy (that is, better real-time performance, fast correction of filtering errors caused by the initial value), and after completing the iteration of the UKF filtering algorithm with a set number of steps N (the exact number of steps is set according to the actual system), the steady-state judgment is performed.

(2) For steady-state judgment, the algorithm selects the sampling strategy according to the judgment condition formula (16). If formula (16) holds, proportional symmetric sampling is switched.

$$\chi_{k-1} = \left[\hat{X}_{k-1}, \hat{X}_{k-1} + \left(\sqrt{(L+\lambda)P_{X,k-1}}\right), \hat{X}_{k-1} - \left(\sqrt{(L+\lambda)P_{X,k-1}}\right)\right]. \tag{18}$$

If formula (12) is not true, the minimum skewness simplex sampling is used.

$$\begin{aligned} \chi_0^1 &= [0], \\ \chi_1^1 &= \left[-\frac{1}{\sqrt{2W_1}}\right], \\ \chi_2^1 &= \left[\frac{1}{\sqrt{2W_1}}\right], \\ \chi_i^{j+1} &= \begin{cases} \begin{bmatrix} \chi_0^j \\ 0 \end{bmatrix}, & i = 0, \\ \begin{bmatrix} \chi_i^j \\ -\frac{1}{\sqrt{2W_{j+1}}} \end{bmatrix}, & i = 1, \ldots, j, \\ \begin{bmatrix} 0 \\ 1 \\ \sqrt{2W_{j+1}} \end{bmatrix}, & i = j+1, \end{cases} \end{aligned} \tag{19}$$

Since the real-time performance and accuracy of hypersphere simplex sampling are inferior to the previous two sampling strategies, this paper does not use hypersphere simplex sampling. After completing the steady-state judgment, the corresponding UKF filtering iteration is performed, and the optimal state estimate at that moment is output. By repeating the above process, the UKF filter with real-time switching of the sampling strategy can be obtained.

The scale factor α can control the distance from the Sigma point to the center and can affect the error of the higher-order terms of the state estimation. The scale factor β is used to introduce the prior information of the random variable X distribution. If the random variable X obeys a normal distribution, the value of β is 2, which is the best. The scale factor is generally selected based on experience. In the simulation experiment, different scale factors α and β are tried, and the best value is selected according to the filtering result. However, the actual system has some real-time online problems, and it is impossible to carry out relevant experiments and obtain the statistical characteristics of the samples. Therefore, it needs to be updated in real time in a scale factor adaptive manner. The specific process of scaling factor adaptive update is as follows:

3.1. Cost Function Construction. The common way to construct the cost function is the Whitaker update criterion, which is an optimal control strategy in the field of adaptive control. By deriving a specific parameter in the cost function, the relationship between the cost function and the parameter is obtained. In this way, an adaptive law for adjusting this parameter is obtained. Some construction methods update the scale factor by the difference between the estimated state value output during the filtering process and the actual measured value. The error expression between the estimated state value and the measured true value is

$$e_k = \frac{1}{N} \sum_{i=k+N+1}^{k} \varepsilon_i \cdot \varepsilon_i^T. \tag{20}$$

In the formula, N controls the mean value of error, and the larger the value, the more stable the mean error value. $\varepsilon_i = z_i - \hat{z}_i$ is the residual vector, z_i is the true value of the measurement, and $\hat{z}_i$ is the estimated mean value of the measurement obtained after the state estimation vector is substituted into the transfer function of the measurement equation. The calculation method is

$$\hat{z}_t = h\left(\hat{x}_{ij-1}, v_i\right). \tag{21}$$

In the formula, $\hat{x}_{ij-1}$ is the system state estimation vector at time i, and the corresponding measurement covariance estimation vector is

$$\hat{e}_k = \sum_{i=0}^{2L} W_1^c \cdot \left(Z_k^i - \hat{z}_k\right) \cdot \left(Z_k^i - \hat{z}_k\right)^T + R_k. \tag{22}$$

Therefore, the cost function based on the difference between the state estimate and the measured true value is obtained, as shown as follows:

$$E_k = \mathrm{tr}\left[\left(e_k - \hat{e}_k\right) \cdot \left(e_k - \hat{e}_k\right)^T\right]. \tag{23}$$

Using the scale factor adaptive UKF filter algorithm, the cost function value needs to be the smallest. In addition, the cost function is established based on the distance between the filtered value $\hat{x}_{k|k}$ and the true value $x_{k|k}$, and the construction process is to approximate the distance $d_{k|k}$ between the filtered value $\hat{x}_{k|k}$ and the true value $x_{k|k}$ through the covariance $P_{k|k}$, as shown as follows:

$$\begin{aligned} P_{k|k} &= E\left[\left(x_{k|k} - \hat{x}_{k|k}\right) \cdot \left(x_{k|k} - \hat{x}_{k|k}\right)^T\right], \\ d_{k|k} &\approx \sqrt{tr\left[P_{k|k}\right]}. \end{aligned} \tag{24}$$

The basic idea is to use the neighborhood $O(\hat{x}_{k|k}, d_{k|k})$ of the filtered value of the k -step and the true value as the sampling range of the Sigma point of the $k+1$ -step, so that the distance of the new sampling point to the central mean does not exceed $d_{k|k}$. The expression is

$$\begin{aligned} \alpha_{k+1|k} \cdot d_{\max^0} &= d_{k|k}, \\ d_{\max^0} &= \max\left\{d_i^0, i \in I\right\}. \end{aligned} \tag{25}$$

In the formula, d_i^0 is determined according to the sampling strategy. This paper adopts the minimum skewness simplex sampling, so $d_i^0 = \sqrt{x_i^T s^T s x_i^j}$. I is the set of corresponding sampling points. The value of the scale factor of step $k+1$ can be calculated by formula 25, and the effect of adaptive update of the scale factor can be achieved.

3.2. Scaling Factor Update Criteria. The first cost function construction criterion is Whitaker update criterion, which can be adjusted according to the price scale factor gradient, and the gradient can be adjusted and updated in the positive or negative direction. Its expression is as follows:

$$\alpha_{k-1} = \alpha_k - \gamma \frac{\partial E_k}{\partial \alpha_k} \cdot \Delta t. \tag{26}$$

In the formula, the size of γ controls the convergence speed of the scale factor, and Δt is the system sampling period. Substituting the update formula into the UKF filter equation, the update equation of the scale factor α_k can be obtained.

3.3. Scale Factor Update under the UKF Framework. The scale factor update process to establish the cost function based on the difference between the state estimate and the measured true value is as follows:

The algorithm is initialized as

$$\begin{aligned} \frac{\partial x_0}{\partial \alpha_k} &= 0, \\ \frac{\partial P_0}{\partial \alpha_k} &= 0. \end{aligned} \tag{27}$$

The algorithm uses the minimum skewness simplex sampling to calculate the corresponding Sigma point, as shown as follows:

$$\frac{\partial \chi_{ik-1}^j}{\partial \alpha_k} = \frac{\partial \chi_{ik-1}^j}{\partial \alpha_k} \cdot \sqrt{P_{k-1}} + \chi_{ik-1}^j \cdot \sqrt{\frac{\partial P_{k-1}}{\partial \alpha_k}}. \tag{28}$$

The nonlinear function transfer is

$$\frac{\partial \chi_{k|k-1}}{\partial \alpha_k} = \frac{\partial f}{\partial \chi}|\chi = \chi_{k|k-1} \cdot \frac{\partial \chi_{k-1}}{\partial \alpha_k},$$

$$\frac{\partial \hat{x}_{kk-1}}{\partial \alpha_k} = \sum_{i=0}^{l+1} \frac{\partial W_i^m}{\partial \alpha_k} \cdot \chi_{k-1}^i + W_i^m \cdot \frac{\partial \chi_{kk-1}^i}{\partial \alpha_k},$$

$$\frac{\partial P_{k,k-1}}{\partial \alpha_k} = \sum_{i=0}^{n,+1} \begin{bmatrix} \frac{\partial W_i^{(c)}}{\partial \alpha_k} \cdot \left(\chi_{k,k-1}{}' - \hat{x}_{k,k-1}\right)\left(\chi_{k,k-1}{}' - \hat{x}_{k,k-1}\right)^T \\ +W_i^{(c)} \cdot \left(\frac{\partial \chi_{k,k-1}{}'}{\partial \alpha_k} - \frac{\partial \hat{x}_{k,k-1}}{\partial \alpha_k}\right)\left(\chi_{k,k-1}^i - \hat{x}_{k,k-1}\right)^r \\ +W_i^{(c)} \cdot \left(\chi_{k,k-1}^i - \hat{x}_{k,k-1}\left(\frac{\partial \chi_{k,k-1}^i}{\partial \alpha_k} - \frac{\partial \hat{x}_{k,k-1}}{\partial \alpha_k}\right)^T\right. \end{bmatrix}, \tag{29}$$

$$\chi_{k,k-1}^{(z)} = \sqrt{P_{k,k-1}} + \chi_{i,k,k-1}^{(z),J} \sqrt{\frac{\partial P_{k,k-1}}{\partial \alpha_k}},$$

$$\frac{\partial Z_k}{\partial \alpha_k} = \frac{\partial h}{\partial \chi}|\chi = \chi_{k,k-1}^{(z)} \cdot \frac{\partial \chi_{k,k-1}^{(z)}}{\partial \alpha_k}.$$

The predicted value gradient of the measurement equation is

$$\frac{\partial \hat{z}_k}{\partial \alpha_k} = \sum_{i=0}^{L+1} W_i^m \cdot \frac{\partial Z_k^i}{\partial \alpha_k}. \tag{30}$$

The algorithm update equation is calculated as

$$\frac{\partial P_{x_i \hat{z}}}{\partial \alpha_k} = \begin{bmatrix} \sum_{i=0}^{n_x+1}\left[\frac{\partial W_i^{(c)}}{\partial \alpha_k} \cdot \left(\chi_{k,k-1}^i - \hat{x}_{k,k-1}\right) \cdot \left(Z_k^{(i)} - \hat{z}_k\right)^r\right] \\ + \sum_{i=0}^{n_x+1} W_i^{(c)} \cdot \left(\frac{\partial \chi_{k,k-1}^i}{\partial \alpha_k} - \frac{\partial}{\partial \alpha_k}\hat{x}_{k,k-1}\right) \cdot \left(Z_k^{(i)} - \hat{z}_k\right)^T \\ + \sum_{i=0}^{n_x+1} W_i^{(c)} \cdot \left(Z_k^{(i)} - \hat{z}_k\right) \cdot \left(\frac{\partial \chi_{k,k-1}^i}{\partial \alpha_k} - \frac{\partial \hat{x}_{k,k-1}}{\partial \alpha_k}\right)^T \end{bmatrix},$$

$$\frac{\partial P_{x_k z_k}}{\partial \alpha_k} = \begin{bmatrix} \sum_{i=0}^{n_x+1} W_i^{(c)} \cdot \left(\frac{\partial Z_k^{(i)}}{\partial \alpha_k} - \frac{\partial \hat{z}_k}{\partial \alpha_k}\right) \cdot \left(Z_k^{(i)} - \hat{z}_k\right)^T \\ + \sum_{i=0}^{n_x+1} W_i^{(c)} \cdot \left(Z_k^{(i)} - \hat{z}_k\right) \cdot \left(\frac{\partial Z_k^{(i)}}{\partial \alpha_k} - \frac{\partial \hat{z}_k}{\partial \alpha_k}\right)^T \end{bmatrix},$$

$$\frac{\partial K}{\partial \alpha_k} = \frac{\partial P_{x_k z_k}}{\partial \alpha_k} P_{z_k}^{-1} - P_{x_k z_k} \cdot \frac{\partial P_{z_k}^{-1}}{\partial \alpha_k},$$

$$\frac{\partial K}{\partial \alpha_k} = \frac{\partial P_{k,k-1}}{\partial \alpha_k} - \frac{\partial K}{\partial \alpha_k} P_{z_k}^T - K_k\left(\frac{\partial P_{z_k}}{\partial \alpha_k}\right)^T. \tag{31}$$

The above is the adaptive update calculation method of the scale factor based on the difference between the state estimation value and the measured true value according to the Whitaker update criterion.

The update process of establishing the cost function based on the distance between the filtered value $\hat{x}_{k|k}$ and the true value $x_{k|k}$ is as follows:

The algorithm selects the minimum skewness simplex sampling and uses $\hat{x}_{k|k}$ and $P_{k|k}$ to calculate the corresponding Sigma point set and weight.

The algorithm calculates $d_{\max^0}, d_{k|k} \approx \sqrt{\mathrm{tr}[P_{k|k}]}$ and sets α as

$$\alpha = \max\left\{\frac{d_{k|k}}{d_{\max^0}}, 10^{-4}\right\},$$
$$\alpha_{k+1|k} \cdot d_{\max^0} = d_{k|k}. \tag{32}$$

Substituting the α obtained above into the iteration of the UKF filtering algorithm, the UKF filtering algorithm with adaptive scale factor is obtained.

4. Research on Optimization Control Method of Tennis Racket String Diameter Based on Kalman Filter Algorithm

As shown in Figure 1, the mass distribution of the tennis racket frame is adjusted by changing the thickness of the throat and the frame of the head and the density of the handle, so that the mass distribution of the tennis racket frame meets the requirements of the International Tennis

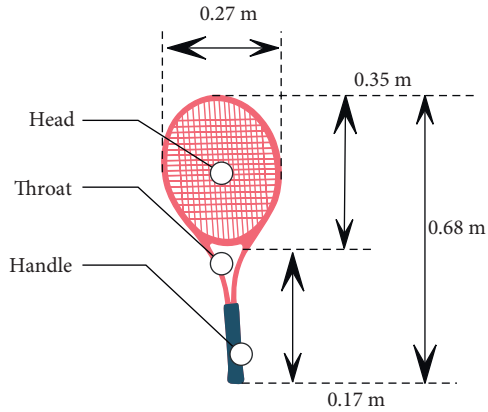

Figure 1: The finite element model of a tennis racket.

Federation for tennis rackets. By colliding a tennis ball with a free-hanging tennis racket, the experimental results show that the finite element model can effectively reflect the speed change of the tennis ball and the deformation state of the tennis racket during the collision.

The vibration of the tennis racket surface is excited by a vibrator with a force sensor. The laser Doppler vibrometer measures the vibration shape of the tennis racket, providing a modal analysis method for the tennis racket vibration research, as shown in Figure 2.

The purpose of using the two-dimensional step function is to express that the deformation area of the tennis racket surface is divided into the maximum deformation area within the force range of the elliptical disk and the logarithmic curve area from the edge of the elliptical disk to the edge of the tennis racket surface after the tennis racket surface is subjected to an external force. Figure 3 shows the 3D model simulation diagram.

The test data of this paper are shown in Table 1, 2:

There is no significant difference between 16L polyester string group and 16L nylon imitation gut string group ($P = 0.530$). This shows that the 16L polyester string and 16L nylon imitation gut string have no significant impact on the speed of the ball, as shown in Figure 4. There is no significant difference between the controllability of 16L polyester string group and 16L nylon imitation gut string group ($P = 0.398$). Therefore, the 16L polyester string and 16L nylon imitation gut string does not show a significant impact on the accuracy of hitting, as shown in Figure 5.

An acceleration sensor is attached to the neck of the tennis racket to test the vibration signal of the racket during the shot. Through the computer YSV engineering test and signal analysis software acquisition system, data is extracted from the racket acceleration signal measured when the ball is hit. This paper uses the acceleration signal of the Z axis for research and analysis. The Z axis is perpendicular to the direction of the racket surface, and the signal collected during the experiment is the most obvious.

The difference in the vibration frequency of the racket acceleration caused by the material of the tennis racket string is shown in Table 3, 4, and Figures 6 and 7.

There is no significant difference in the impact vibration frequency between 16L polyester string group and 16L nylon imitation gut string group ($P = 0.082$). It shows that the 16L polyester string and 16L nylon imitation gut do not have much influence on the vibration frequency of the racquet collision. There is no significant difference in swing frequency between 16L polyester thread string group and 16L nylon imitation string group ($P = 0.189$). It shows that 16L polyester thread and 16L nylon imitation gut thread do not have much influence on the swing vibration frequency.

The difference in the vibration frequency of the racket acceleration caused by the string diameter of the tennis racket is shown in Table 5, 6, Figure 8, and 9.

There is no significant difference between the impact vibration frequency 16L polyester string group and NO. 18 polyester string group. This shows that the string diameter of the tennis string made of 16L polyester string and 1 NO. 18 polyester string does not have much influence on the vibration frequency of the racket collision. There is no significant difference between the swing frequency of the string diameter thick line and the thin line. It shows that the string diameter 16L polyester string and the NO. 18 polyester string do not have much influence on the vibration frequency of the swing.

Through the above research, the optimization control method of tennis racket string diameter is analyzed, and it is verified that the Kalman filter algorithm can play a certain role in the optimization control of tennis racket string diameter.

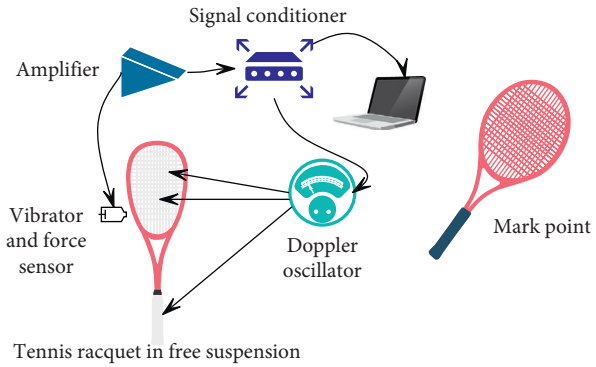

Figure 2: Tennis racket vibration mode test system.

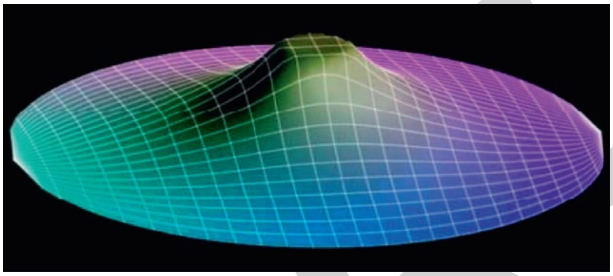

Figure 3: Force and deformation diagram of tennis racket surface.

Table 1: The speed and control score of different material groups.

NO	16L polyester thread	16L nylon imitation gut	NO	16L polyester thread	16L nylon imitation gut	NO	16L polyester thread	16L nylon imitation gut
1	105.16	104.45	17	101.71	101.25	33	118.21	103.35
2	105.84	102.42	18	100.27	115.76	34	106.25	104.76
3	110.81	108.09	19	110.01	107.51	35	105.26	100.20
4	113.46	98.92	20	113.58	97.00	36	118.52	102.41
5	104.02	99.34	21	104.29	100.00	37	104.87	105.54
6	102.36	105.78	22	118.09	101.86	38	108.94	112.88
7	100.19	107.17	23	114.08	110.60	39	104.53	110.46
8	111.09	115.57	24	118.83	102.46	40	109.35	116.20
9	102.31	113.70	25	100.27	107.58	41	115.93	112.70
10	101.15	105.89	26	109.85	108.01	42	118.08	109.40
11	112.51	113.80	27	107.89	108.46	43	101.42	108.06
12	100.22	110.68	28	113.63	109.02	44	112.92	102.42
13	104.82	99.30	29	113.86	100.70	45	111.91	113.30
14	103.74	107.76	30	118.19	114.16	46	117.28	110.26
15	115.48	98.46	31	111.35	100.59	47	113.90	108.37
16	108.65	110.35	32	103.67	112.77	48	102.69	105.15

Table 2: The control score of different material groups.

NO	16L polyester thread	16L nylon imitation gut	NO	16L polyester thread	16L nylon imitation gut	NO	16L polyester thread	16L nylon imitation gut
1	4.55	5.11	17	4.76	4.25	33	5.78	4.34
2	5.44	5.55	18	4.92	5.03	34	4.91	3.92
3	4.50	4.30	19	5.39	4.57	35	5.66	5.44
4	5.31	4.47	20	4.71	4.49	36	5.15	4.31
5	5.38	5.62	21	4.58	3.93	37	5.04	5.26
6	5.74	5.26	22	5.81	5.26	38	5.23	5.49
7	5.37	5.38	23	5.74	4.24	39	5.11	4.33
8	4.54	4.71	24	5.68	4.85	40	4.85	5.43
9	4.89	5.27	25	5.21	4.11	41	5.22	4.75
10	4.79	5.44	26	5.24	5.08	42	4.82	4.27
11	5.17	5.35	27	5.02	4.66	43	4.76	4.07
12	5.02	4.82	28	4.56	5.13	44	4.35	4.48
13	4.68	4.41	29	5.60	5.44	45	5.74	3.88
14	4.53	5.02	30	5.85	5.20	46	5.83	4.19
15	4.50	5.64	31	5.00	5.13	47	4.45	5.07
16	4.50	4.03	32	4.61	4.60	48	4.93	4.49

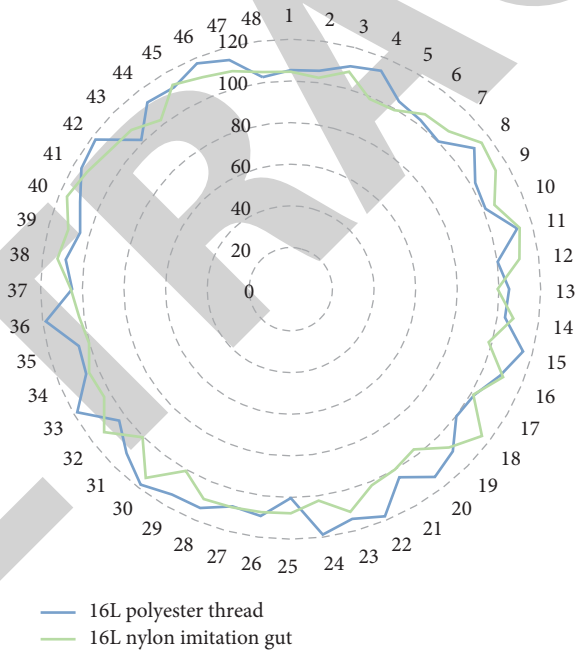

Figure 4: The speed of different material groups.

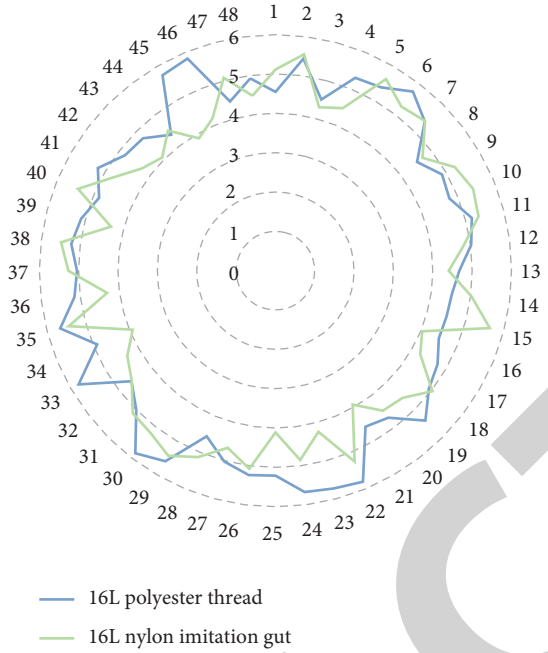

Figure 5: The statistical diagram of the control score of different material groups.

Table 3: Racket impact vibration frequencies of different material groups.

NO	16L polyester thread	16L nylon imitation gut	NO	16L polyester thread	16L nylon imitation gut	NO	16L polyester thread	16L nylon imitation gut
1	118.76	111.01	17	119.92	110.37	33	114.54	117.31
2	101.48	110.97	18	110.53	122.05	34	109.93	110.77
3	107.52	123.90	19	110.75	123.13	35	111.92	121.02
4	111.76	120.39	20	100.66	116.58	36	107.35	119.23
5	112.50	122.81	21	119.21	112.36	37	119.45	118.73
6	100.97	111.74	22	113.74	120.55	38	113.38	118.70
7	104.30	120.30	23	118.33	121.93	39	110.41	110.30
8	117.69	121.96	24	114.85	116.18	40	102.75	111.01
9	104.34	114.88	25	111.22	110.43	41	102.88	113.04
10	108.07	120.25	26	107.05	110.01	42	101.31	119.13
11	109.05	122.45	27	111.91	114.90	43	113.96	109.87
12	106.44	109.83	28	99.95	112.64	44	109.34	111.13
13	108.42	121.65	29	100.56	123.12	45	116.36	115.13
14	110.10	110.64	30	103.13	120.64	46	99.79	112.45
15	112.14	122.29	31	99.23	118.40	47	100.69	116.89
16	102.73	122.99	32	114.30	117.69	48	119.80	116.60

Table 4: Swing vibration frequency of different material groups.

NO	16L polyester thread	16L nylon imitation gut	NO	16L polyester thread	16L nylon imitation gut	NO	16L polyester thread	16L nylon imitation gut
1	4.36	5.88	17	5.76	5.75	33	5.80	4.70
2	5.46	5.56	18	4.62	4.91	34	5.63	6.20
3	5.26	5.24	19	5.56	5.40	35	5.47	5.86
4	5.25	4.92	20	5.62	5.44	36	5.55	5.40
5	5.30	5.84	21	5.77	5.42	37	5.87	6.08
6	5.03	5.86	22	4.92	5.28	38	5.58	4.88
7	4.81	5.63	23	5.56	4.72	39	4.62	5.17
8	4.83	5.97	24	4.41	5.12	40	4.62	6.06
9	4.80	5.67	25	5.06	5.28	41	5.00	4.72

Table 4: Continued.

NO	16L polyester thread	16L nylon imitation gut	NO	16L polyester thread	16L nylon imitation gut	NO	16L polyester thread	16L nylon imitation gut
10	5.28	5.25	26	4.75	6.05	42	5.00	6.28
11	4.80	4.92	27	4.53	5.75	43	5.28	5.98
12	4.43	5.08	28	5.85	5.37	44	5.83	4.74
13	5.14	5.15	29	5.49	4.79	45	5.21	5.11
14	5.63	5.16	30	5.49	4.85	46	4.84	4.91
15	4.77	5.08	31	4.55	6.23	47	5.74	5.74
16	4.92	5.32	32	4.86	4.92	48	4.39	5.11

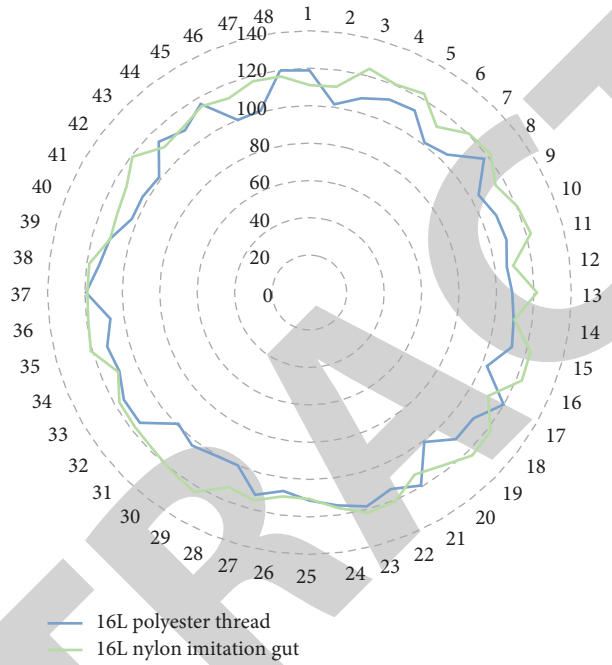

Figure 6: Statistical diagram of racket impact vibration frequencies of different material groups.

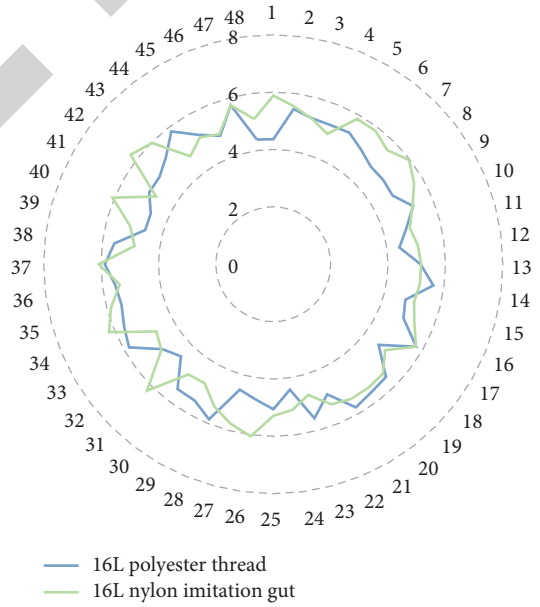

Figure 7: Statistical diagram of swing frequency of different material groups.

Table 5: The vibration frequency of the racket acceleration and impact of different string diameter groups.

NO	16L polyester thread	No. 18 polyester thread	NO	16L polyester thread	No. 18 polyester thread	NO	16L polyester thread	No. 18 polyester thread
1	37.88	38.2	17	38.14	38.2	33	37.97	38.2
2	37.44	38.2	18	37.83	38.2	34	38.02	38.2
3	37.89	38.2	19	37.90	38.2	35	37.49	38.2
4	37.60	38.2	20	37.56	38.2	36	37.80	38.2
5	37.42	38.2	21	37.77	38.2	37	37.95	38.2
6	38.05	38.2	22	37.99	38.2	38	37.78	38.2
7	37.34	38.2	23	38.08	38.2	39	37.59	38.2
8	37.52	38.2	24	38.15	38.2	40	37.62	38.2
9	37.91	38.2	25	37.92	38.2	41	38.13	38.2
10	38.02	38.2	26	38.11	38.2	42	38.01	38.2
11	37.40	38.2	27	37.68	38.2	43	37.89	38.2
12	37.87	38.2	28	37.51	38.2	44	37.93	38.2
13	37.86	38.2	29	37.63	38.2	45	37.69	38.2
14	37.38	38.2	30	37.85	38.2	46	37.87	38.2
15	37.70	38.2	31	38.19	38.2	47	37.51	38.2
16	37.67	38.2	32	37.35	38.2	48	38.02	38.2

Table 6: Vibration frequency of racket swing in different string diameter groups.

NO	16L polyester thread	No. 18 polyester thread	NO	16L polyester thread	No. 18 polyester thread	NO	16L polyester thread	No. 18 polyester thread
1	40.13	40.66	17	39.87	40.56	33	40.83	39.94
2	40.52	39.71	18	40.58	39.87	34	40.70	40.00
3	39.96	39.95	19	40.77	40.26	35	40.25	39.90
4	40.13	40.24	20	39.97	39.72	36	40.05	39.71
5	40.19	40.36	21	40.15	39.63	37	40.40	39.95
6	40.39	40.00	22	40.54	39.77	38	40.26	40.41
7	40.55	39.89	23	40.49	39.98	39	39.93	39.76
8	40.78	40.07	24	40.40	40.07	40	39.99	40.42
9	40.15	40.11	25	40.54	40.10	41	39.91	40.67
10	40.23	39.73	26	40.05	39.88	42	40.69	40.09
11	40.70	39.81	27	39.95	39.61	43	40.24	40.24
12	40.26	40.11	28	40.60	40.01	44	40.37	39.80
13	40.59	40.01	29	40.30	40.53	45	40.26	39.80
14	40.54	40.11	30	39.97	40.02	46	40.26	40.58
15	40.21	40.35	31	40.69	40.11	47	40.84	39.99
16	40.46	40.09	32	40.29	40.26	48	40.10	39.95

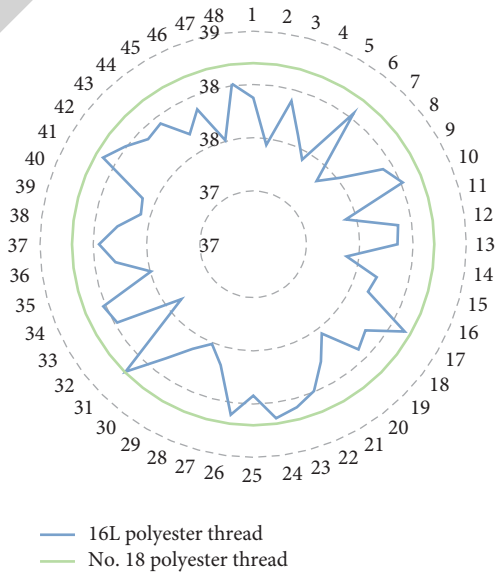

Figure 8: The statistical diagram of the vibration frequency of the racket acceleration and impact of different string diameter groups.

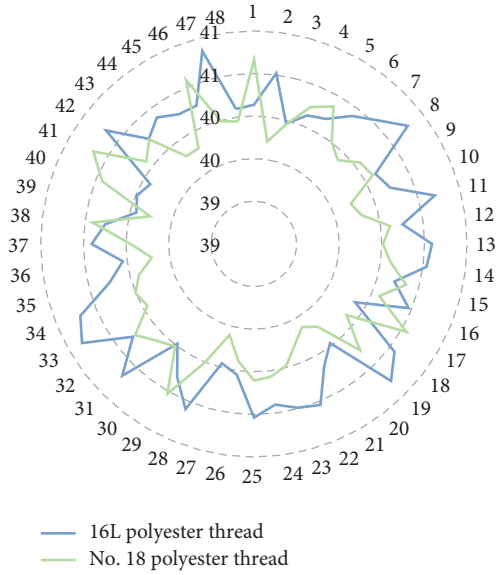

Figure 9: Statistical graphs of vibration frequency of racket swing in different string diameter groups.

5. Conclusion

Tennis players' own technical movements have a direct impact on the ball hitting effect and arm load. However, in addition to this, the performance of the racket also has a significant impact on the hitting effect and arm load. That is to say, the racket parameters that determine the performance of the racket have a significant impact on the hitting effect and arm load. As an important parameter of the racket, the mass distribution of the tennis racket is closely related to the swing weight and force of the racket. The change in mass distribution will cause a series of chain reactions, which will ultimately change the performance of the racket and affect the impact of the ball and the impact load of the racket on the arm when hitting the ball. This paper combines the Kalman filter algorithm to study the optimization control method of tennis racket string diameter and improves the research effect through the intelligent simulation system. Moreover, this paper systematically studied the optimization control method of tennis racket string diameter and verified that the Kalman filter algorithm can play a certain role in the optimization control of tennis racket string diameter.

Data Availability

The labeled dataset used to support the findings of this study are available from the corresponding author upon request.

Conflicts of Interest

The author declares no competing interests.

Acknowledgments

This study was sponsored by Shenyang Jianzhu University.

References

[1] L. YanRu, "An artificial intelligence and machine vision based evaluation of physical education teaching," *Journal of Intelligent and Fuzzy Systems*, vol. 40, pp. 1–11, 2020.

[2] J. P. R. Lara, C. L. R. Vieira, and M. S. Misuta, "Validation of a video-based system for automatic tracking of tennis players," *International Journal of Performance Analysis in Sport*, vol. 18, no. 1, pp. 137–150, 2018.

[3] G. Tsagkatakis, M. Jaber, and P. Tsakalides, "Convolutional neural networks for the analysis of broadcasted tennis games," *Electronic Imaging*, vol. 2018, no. 2, pp. 1–6, 2018.

[4] T. Fernando, S. Denman, S. Sridharan, and C. Fookes, "Memory augmented deep generative models for forecasting the next shot location in tennis," *IEEE Transactions on Knowledge and Data Engineering*, vol. 32, no. 9, pp. 1785–1797, 2019.

[5] N. Elliott, S. Choppin, S. Goodwill, T. Senior, J. Hart, and T. Allen, "Single view silhouette fitting techniques for estimating tennis racket position," *Sports Engineering*, vol. 21, no. 2, pp. 137–147, 2018.

[6] S. A. Kovalchik, J. Sackmann, and M. Reid, "Player official or machine? uses of the challenge system in professional tennis," *International Journal of Performance Analysis in Sport*, vol. 17, no. 6, pp. 961–969, 2017.

[7] B. Giles, S. Kovalchik, and M. Reid, "A machine learning approach for automatic detection and classification of changes of direction from player tracking data in professional tennis," *Journal of Sports Sciences*, vol. 38, no. 1, pp. 106–113, 2020.

[8] M. R. Keyvanpour, S. Vahidian, and M. Ramezani, "HMR-vid: a comparative analytical survey on human motion recognition in video data," *Multimedia Tools and Applications*, vol. 79, no. 43, Article ID 31819, 2020.

[9] Y. F. Ji, J. W. Zhang, Z. Shi, M.-H. Liu, and J. Ren, "Research on real–time tracking of table tennis ball based on machine learning with low-speed camera," *Systems Science & Control Engineering*, vol. 6, no. 1, pp. 71–79, 2018.

[10] E. E. Cust, A. J. Sweeting, K. Ball, and S. Robertson, "Machine and deep learning for sport-specific movement recognition: a systematic review of model development and performance," *Journal of Sports Sciences*, vol. 37, no. 5, pp. 568–600, 2019.

[11] R. Gayanov, K. Mironov, R. Mukhametshin, and A. Vokhmintsev, "Transportation of small objects by robotic throwing and catching: applying genetic programming for trajectory estimation," *IFAC-PapersOnLine*, vol. 51, no. 30, pp. 533–537, 2018.

[12] J. Zhang, H. Yu, H. Deng, Z. Chai, M. Ma, and X. Zhong, "A robust and rapid camera calibration method by one captured image," *IEEE Transactions on Instrumentation and Measurement*, vol. 68, no. 10, pp. 4112–4121, 2018.

[13] O. Cant, S. Kovalchik, R. Cross, and M. Reid, "Validation of ball spin estimates in tennis from multi-camera tracking data," *Journal of Sports Sciences*, vol. 38, no. 3, pp. 296–303, 2020.

[14] M. R. Mohammadi, "Deep multiple instance learning for airplane detection in high-resolution imagery," *Machine Vision and Applications*, vol. 32, no. 1, pp. 1–14, 2021.

[15] Y. Zhao, R. Xiong, and Y. Zhang, "Model based motion state estimation and trajectory prediction of spinning ball for ping-pong robots using expectation-maximization algorithm," *Journal of Intelligent and Robotic Systems*, vol. 87, no. 3, pp. 407–423, 2017.

[16] M. F. López, "Research on the specific movement of the head in tennis strokes," *ITF Coaching & Sport Science Review*, vol. 28, no. 80, pp. 16–19, 2020.